ISSN: 2688-8645

Comparative Study on Sealing Performance of 2D and 3D Models for Pressurized Cable Crown Sheave

Zebing Wu, Xiaochun Zhu, Kenan Liu, Zihao Zhang, Yifei Lin

College of Mechanical Engineering, Xi'an Shiyou University, Xi'an Shaanxi, 710065, China

Abstract

To address the seal failure and leakage problems of the pressurized cable crown sheave operating under high-pressure conditions of 35–50 MPa, 2D and 3D solid finite element models (FEMs) for the main sealing structure were established to investigate the sealing performance of the O-ring seal.As the fluid pressure increased to 50 MPa, the von Mises equivalent stress of the O-ring reached 16.588 MPa, which is close to the allowable stress limit of the material. Beyond this pressure threshold, the region with the maximum equivalent stress is prone to tearing, leading to seal failure.Three-dimensional FEM analysis was conducted to characterize the deformation, equivalent stress and contact pressure behaviors of the O-ring. The results show that the mechanical response of the O-ring is consistent with the predictions of the 2D axial propulsion model, which verifies the effectiveness of the 2D model under symmetric loading conditions.However, for scenarios involving O-ring twisting or asymmetric loading, 3D FEM analysis is indispensable to obtain accurate simulation results.This study provides a valuable reference for the sealing design of similar sealing structures in engineering applications.

Keywords

Pulley under Pressure; Sealing Ring; Three-Dimensional Model; Stress Concentration.

1. Introduction

To comply with the development trend of petroleum extraction technology in China and meet the requirements of low-cost and high-efficiency pressurized operations, a new type of pressurized cable crown sheave with dual functions of pressure-bearing and guiding has emerged as the times require, and its geometric structure is shown in Figure 1

Fig 1. Pressure-bearing pulley geometry

The core of this equipment lies in its sealing system, which must operate reliably under a high-pressure environment of 35–50 MPa. Its failure will directly lead to the loss of equipment functions and even cause serious safety accidents. Therefore, the design and research of the sealing structure have become the key to ensuring the safe and reliable operation of the equipment. As a core sealing component in the mechanical field, the O-ring seal realizes the

ISSN: 2688-8645

initial sealing force through extrusion deformation generated by contact with the shell. Based on this principle, the pressurized cable crown sheave adopts O-rings to construct its core sealing structure, thus ensuring reliable sealing and pressurized operations under high-pressure working conditions [1].

Tan Jing, Guan Wenjin, and other researchers investigated the influence of different parameters on the sealing performance of O-rings by using ANSYS and ABAQUS, respectively [2-3]. Zhang Jing et al. conducted a finite element analysis on the contact pressure of O-rings [4]. Yang Bo, Wu Zebing, and their colleagues studied the sealing stress of O-rings under eccentric working conditions [5-6]. On this basis, this paper first analyzes the fundamental cause of O-ring failure (extrusion phenomenon) based on the sealing principle. The ANSYS finite element analysis software was used to establish a 2D axisymmetric model and a 3D solid model of the sealing structure, respectively. The nonlinear finite element method was adopted to simulate the deformation and stress states of O-rings under different medium pressures. This study compares the differences between the 2D and 3D models, clarifies the advantages of the 3D model in capturing local deformation details and reflecting the actual state of the sealing interface, and verifies the applicability of the 2D model in preliminary analysis

2. Mechanical Performance Analysis and Sealing Principle of O-rings

2.1. Mechanical Performance Analysis and Sealing Principle of O-rings

Sealing rings achieve the sealing effect by means of compressed elastomers, and their operating mechanism consists of two stages: first, the installation pre-compression causes the sealing ring to undergo elastic deformation to generate an initial contact pressure; second, under the action of the working fluid pressure, the sealing ring deforms further to produce a self-reinforcing effect [7]. This dual-action mechanism means that compressed elastomer seals are inherently self-reinforced seals.

When the sealing ring is subjected to the fluid pressure P1, the resulting contact pressure is expressed as:

$$P_c = P_{co} + \Delta P_c = P_{co} + kP_1 = P_{co} + v/(1-v)P_1 \quad (1)$$

Where:

P_c—total system contact pressure, representing the comprehensive pressing force at the sealing interface under the action of fluid pressure, in MPa;

P_{co}—initial pre-contact pressure, referring to the static contact stress generated by the compression of the sealing ring during the assembly stage, in MPa;

ΔP_c—fluid-induced contact pressure, which is the coupled compressive stress transmitted from the working fluid pressure to the sealing interface through the seal material, in MPa.

In the expression for ΔPc, k denotes the lateral pressure coefficient. For rubber seals, the value of k is approximately 1. v represents the Poisson's ratio of the rubber sealing ring, and for rubber seals, the value of v is roughly 0.5.

To maintain an effective seal, it is essential to ensure that $P_c > P_1$. Since ΔPc is always less than P1, a sufficient initial pre-contact pressure P_{co} must be maintained. In other words, the sealing ring must have an adequate pre-compression ratio to guarantee reliable sealing [8].

2.2. Seal Compression Ratio

O-ring seals are typical squeeze-type seals. Regarding the conventional compression ratio ε, different sealing types correspond to different value ranges:For cylindrical static seals and reciprocating dynamic seals, the conventional range of ε is 10%–15%;For flat-face static seals, ε should be controlled within the range of 15%–30%;For rotary dynamic seals, the conventional value range of ε is 3%–8%;For low-friction seals, the conventional range of the

ISSN: 2688-8645

compression ratio ε is 5%–8%.As shown in Figure 2, ε is generally expressed by the following formula:

$$\varepsilon = \frac{d_0 - h_0}{d_0} \times 100\% \quad (2)$$

Where:

h_0 is distance from the bottom of the seal groove to the sealed surface, in mm;

d_0 is outer diameter of the sealing ring, in mm.

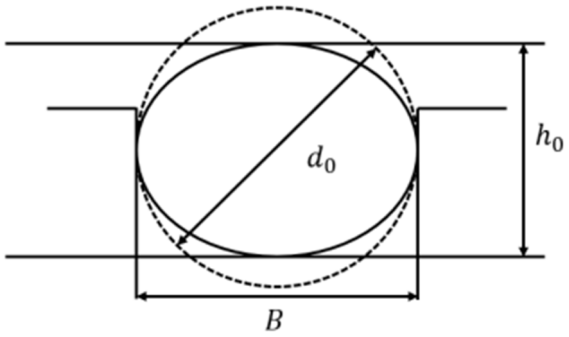

Fig 2. Seal ring compression ratio

According to the aforementioned Formula (2), the compression ratio of the sealing ring is calculated to be 22.64%, which falls within the range of 15%–30% and thus meets the selection requirements.

After the sealing ring is fitted onto the seal groove, a certain amount of elongation is generally generated. To prevent the sealing ring from being too loose after installation in the seal groove, the elongation can be set at a slightly larger value. Therefore, a certain amount of contact pressure is also generated between the sealing ring and the seal groove due to the interference fit.

Based on the aforementioned working principle of the O-ring seal, it can be inferred that the failure of the O-ring seal may be attributed to the unreasonable design of its compression ratio and elongation. Hence, in the subsequent finite element analysis, the pre-contact pressure and stress induced by the compression and elongation of the sealing ring should be taken into consideration.

3. Establishment of the Finite Element Model

3.1. Establishment of the Finite Element Model for the Sealing Structure

This structure consists of a polytetrafluoroethylene (PTFE) retainer ring, a rubber O-ring, an outer shell, and an inner shell, with the specific geometric parameters listed in Table 1.

Figure 3 shows the finite element analysis model for radial compression, which simplifies the assembly process and only considers the pre-compression process of the O-ring.

Table 1. Geometric Parameters of Pressure-Sealed Pulley Sealing Rings

Parameters	Numble /mm
O-ring structural dimension d0	Φ320×5.3
rectangular groove width B	9.8
rectangular groove depth H	4.1
rectangular sealing retainer ring height h	4.1
rectangular sealing retainer ring thickness b	3

ISSN: 2688-8645

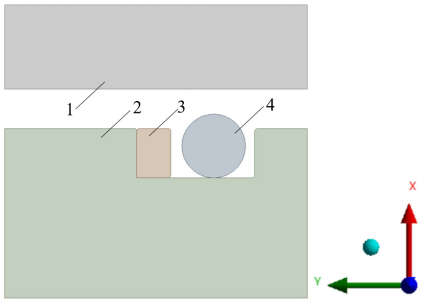

1-Outer shell 2-Inner shell 3-Rectangular retainer ring 4-Seal ring

Fig 3. Radial compression finite element analysis model

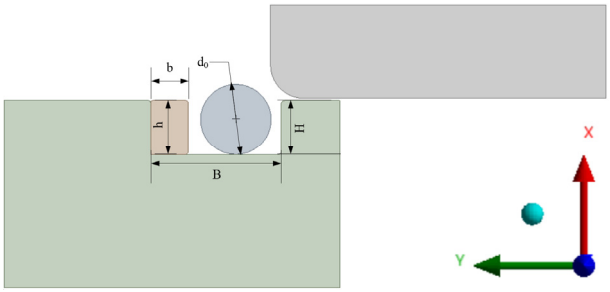

Fig 4. Axial propulsion finite element analysis model

Figure 4 shows the axial propulsion finite element analysis model, which takes into account the process of fitting the inner shell into the outer shell .

3.2. Material Parameters

In the mentioned sealing structure, the materials of each component and their mechanical properties are defined as follows:The outer shell and groove components are made of titanium alloy TC4, which has high stiffness characteristics with an elastic modulus of 110 GPa and a Poisson's ratio of 0.34.The sealing retainer ring is made of polytetrafluoroethylene (PTFE), with an elastic modulus of 960 MPa and a Poisson's ratio of 0.45.The O-ring seal is made of hydrogenated nitrile butadiene rubber (HNBR) with a Shore hardness of 90 HA. It exhibits significant hyperelastic behavior in terms of mechanics. To accurately simulate the complex mechanical response during the sealing process, material nonlinearity, large geometric deformation and contact boundary nonlinearity need to be considered simultaneously.For rubber-like physically nonlinear materials, the Mooney-Rivlin model is generally selected for characterization.

$$W\left(I_1, I_2\right) = \sum_{i,j=0}^{n} C_{ij}\left(I_1 - 3\right)^i \left(I_2 - 3\right)^j \tag{3}$$

Where:

W is strain energy density;

Cij is Rivlin coefficients;

I1, I2 is the first and second Green strain invariants, respectively.

A two-parameter Mooney-Rivlin model is adopted in this paper, and thus the above equation can be rewritten as:

$$W = C_{10}\left(I_1 - 3\right) + C_{01}\left(I_2 - 3\right) \tag{4}$$

Where C_{10} and C_{01} are material coefficients. According to the method for determining the rubber material constants in Reference, the Poisson's ratio of the rubber material in this paper is set to 0.5, and thus C_{10} and C_{01} are determined to be 2.79 MPa and 0.7 MPa, respectively.

3.3. Mesh Generation and Boundary Conditions

Five contact pairs were established, including those between the O-ring and the outer shell, between the O-ring and the inner shell, as well as between the rectangular retainer ring and the outer shell, inner shell, and O-ring. The contact mode of these five contact pairs was uniformly set as line-to-line contact, and all contact types were categorized as rigid-flexible contact. The generalized Lagrangian method was selected as the solution algorithm for the contact pairs. The friction coefficient between the O-ring and the inner and outer shells was set to 0.1, while

ISSN: 2688-8645

the friction coefficient between the rectangular retainer ring and the inner and outer shells was set to 0.03.

In this paper, under the premise of balancing computational efficiency and accuracy, local mesh refinement was performed on the key contact-prone regions, which ensured high computational accuracy while shortening the calculation time.

The numerical simulation was carried out in three load steps:

Load Step 1: Simulate the installation and stretching process of the O-ring to establish the initial assembly stress state.

Load Step 2: Simulate the outer shell assembly process to achieve pre-compression of the O-ring and form the initial sealing contact pressure.

Load Step 3: Apply the working fluid pressure to simulate the equivalent stress and contact pressure of the O-ring under high-pressure working conditions.

The boundary conditions are as follows:

In all analysis steps, the seal groove was set with fixed constraints.

Displacement loads were applied according to the assembly method.

Radial compression model: Apply a displacement of 3.3 mm along the negative X-axis direction to the outer shell.

Axial propulsion model: Apply a displacement along the positive Y-axis direction to the outer shell to move it to the pre-designed installation position.

In Load Step 3, a pressure load was applied to the surface of the O-ring exposed to the fluid side.

3.4. Several Basic Assumptions

The following assumptions are made for the finite element simulation:

The rubber sealing ring material is regarded as a homogeneous and continuous medium, with its elastic modulus and Poisson's ratio defined as fixed material parameters.

The rubber material exhibits nearly incompressible behavior, and its volume remains unchanged during the deformation process.

The elastic modulus of the outer shell, seal groove and retainer ring structures is much higher than that of the rubber material, so they are simplified as rigid bodies in the model. The entire sealing structure is treated under the condition of ideal axisymmetry in terms of both geometry and load.

4. Analysis of 2D Simulation Results

4.1. Influence of Different Fluid Pressures on Sealing Performance

Figure 5 shows the nephograms of equivalent stress and contact pressure of the O-ring obtained from the analysis of two models, namely radial compression (left) and axial propulsion (right), when the sealing pressure is 35 MPa respectively.

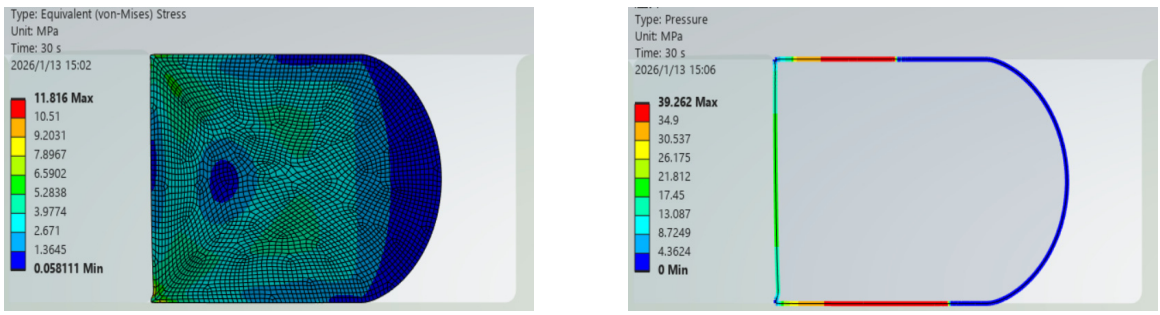

Fig 5. Equivalent stress and contact pressure of the seal ring under 35 MPa pressure

ISSN: 2688-8645

Through the analysis of the contact pressure and equivalent stress nephograms, Figure 6 illustrates the variation laws of equivalent stress and contact pressure with fluid pressure. This figure reflects the pressure distribution of the sealing contact surface under different pressure conditions. The value of contact pressure directly characterizes the sealing performance of the O-ring. When the fluid pressure increases, the contact pressure rises correspondingly, and its peak value remains consistently higher than the fluid pressure. This characteristic not only ensures the reliability of the sealing effect but also embodies the unique self-energizing sealing effect of the O-ring.

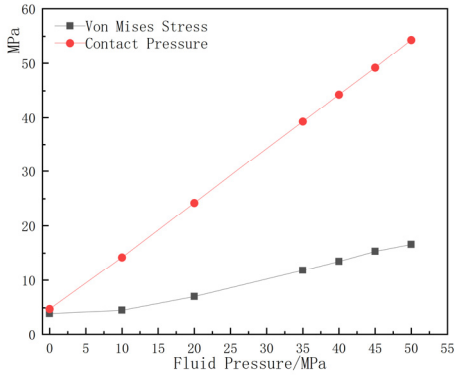

Fig 6. Graph of the relationship between medium pressure, contact pressure and equivalent stress

5. Analysis of 3D Simulation Results

5.1. Geometric Modeling

To efficiently and accurately analyze the assembly and operation processes of this mechanical system, it is necessary to simplify the geometric model based on the working principle of the system. A simplified 3D finite element analysis model was established via SolidWorks software, as shown in Figure 9 below.

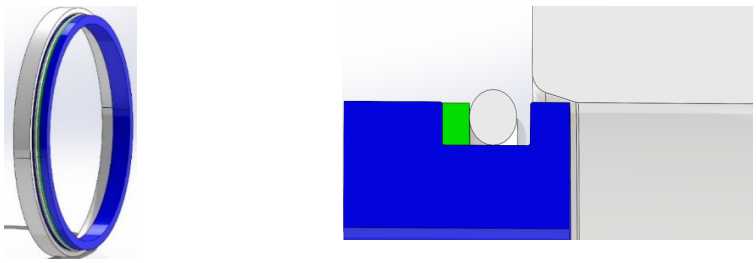

Fig 7. Geometric model for finite element analysis

5.2. Geometric Modeling

The contact pairs, boundary conditions, and load steps were consistent with those of the 2D model.

On the premise of balancing computational efficiency and accuracy, the finite element model was meshed, resulting in a total of 937,687 nodes and 534,593 elements.

5.3. 3D Finite Element Results Analysis

(1) Influence of Different Sealing Medium Pressures on Contact Pressure Distribution

The contact pressure distributions under different sealing medium pressures (35, 40, 45, and 50 MPa) at a compression ratio of 22.64% are illustrated in Figure 10. As the medium pressure increases from 35 MPa to 50 MPa, the measured maximum contact pressure values are 48.342 MPa, 53.518 MPa, 58.77 MPa, and 63.955 MPa, respectively. All peak contact pressures are

ISSN: 2688-8645

higher than the medium pressures under the corresponding working conditions, which verifies that the O-ring can maintain stable sealing performance under various pressure conditions. The law that the maximum contact pressure increases with the rise of medium pressure reveals the mechanical mechanism of the self-enhancing sealing effect of the sealing ring under the preloaded state. From the perspective of pressure field distribution characteristics, the central line region of the sealing ring bears the maximum compressive strain, thus forming the contact pressure extremum region here, and finally presenting a stress distribution pattern with a quasi-parabolic characteristic.

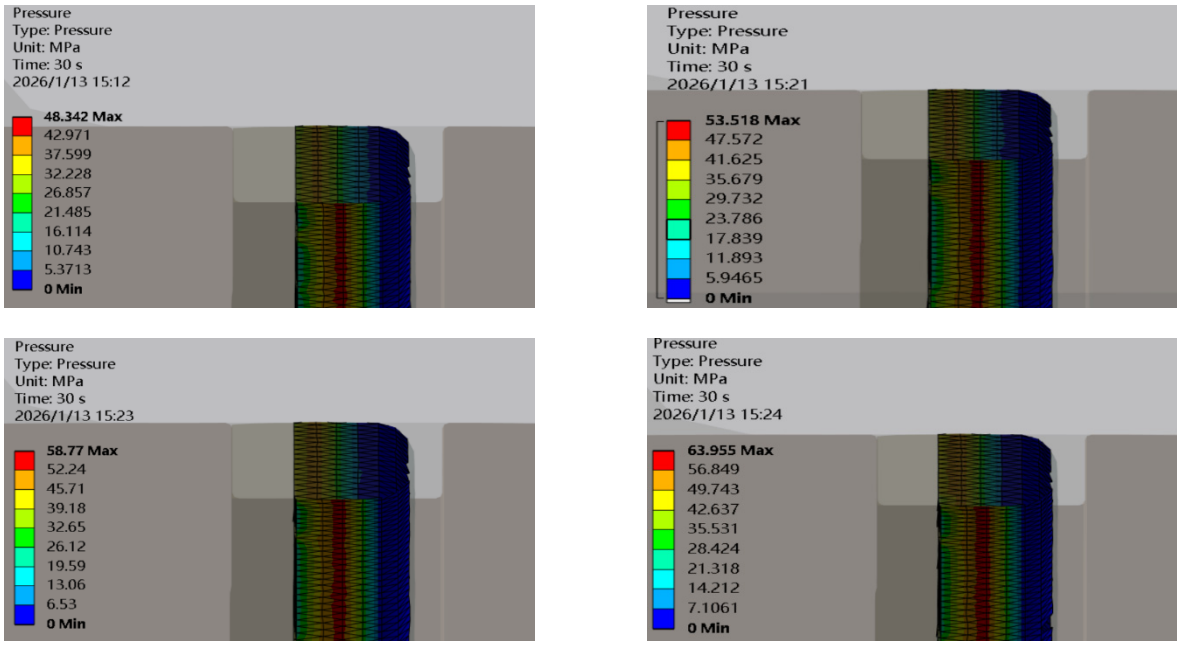

Fig 8. Contact pressure distribution contour map of sealing rings under different medium pressures

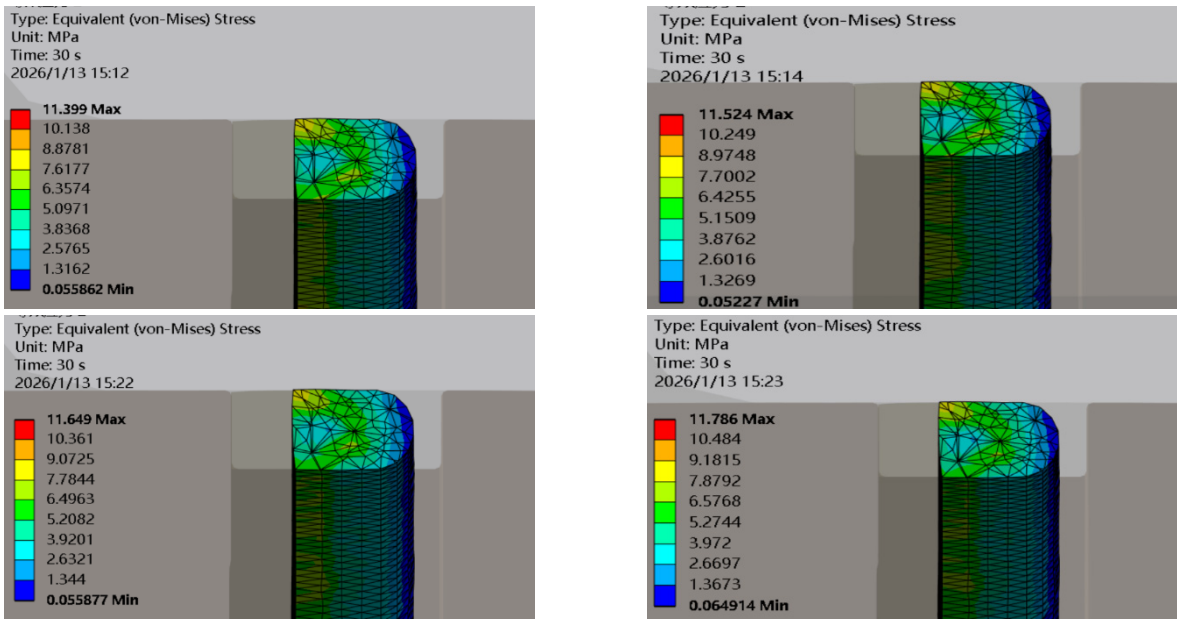

Fig 9. Contour plot of von mises stress in sealing rings under different medium pressures

(2) Influence of Different Sealing Medium Pressures on Equivalent Stress

ISSN: 2688-8645

The equivalent stress distribution results of the sealing ring obtained via ANSYS simulation are illustrated in Figure 11. As the medium pressure increases from 35 MPa to 50 MPa, the measured maximum equivalent stress values are 10.399 MPa, 11.524 MPa, 11.649 MPa, and 11.786 MPa, respectively. With the gradual increase of pressure, the generated equivalent stress increases accordingly. The stress concentration regions expand toward both ends while the area of these regions gradually decreases.

The 2D model simplifies the annular sealing structure into a 2D cross-section passing through the central axis, with all geometric features treated as axisymmetric. This approach neglects the non-axisymmetric details of the actual 3D structure, such as tiny chamfers at the bottom corners of the seal groove, uneven wall thickness of the shells, eccentric installation of the O-ring, and sharp edges of the retainer ring. These details induce local stress concentrations in the 3D model, but such effects are averaged out in the 2D model, leading to an overestimation of the calculated stress values. By contrast, the 3D model retains the annular surface contact of the sealing structure, resulting in a contact area that is more consistent with the actual scenario and a more uniform stress distribution. Meanwhile, the 3D model can capture asymmetric gaps that cannot be reflected in the 2D model, which is a key contributing factor to the uneven stress distribution in the 3D simulation.

All loads applied to the 2D model are axisymmetric relative to the central axis. Under such purely symmetric loading conditions, the stress in the 2D model is generated solely by uniform compression, without additional shear or bending stress. The stress state is simple, and the numerical results are relatively stable. A core advantage of the 3D model lies in its ability to simulate asymmetric loading. In addition to installation stretching, assembly pre-compression, and medium pressure, the 3D model also incorporates the uneven contact pressure caused by asymmetric gaps. After the superposition of multiple sets of asymmetric stresses, the maximum contact pressure is further amplified.

6. Conclusion

Firstly, based on the working principle and geometric structure of the pressurized pulley, this paper established simplified 2D and 3D finite element analysis models by using ANSYS software.

The analysis of the 2D and 3D models under different medium pressures shows that the contact pressure increases synchronously with the medium pressure. Its self-sealing mechanism ensures that the peak contact pressure is always higher than the medium pressure, thus guaranteeing the sealing effectiveness.

The 2D model is suitable for simplified working conditions with symmetric loads and ideal geometries, featuring conservative stress calculations and high computational efficiency. In contrast, the 3D model is applicable to actual working conditions with asymmetric loads and real geometries; it can capture local stress concentrations and additional stresses, yielding results that are more consistent with reality, but at a higher computational cost.

Both models exhibit consistent stress growth trends. The 2D model can be used as an initial reference for the 3D model, while accurate calculations must ultimately be achieved via the 3D model

Acknowledgments

Natural Science Foundation.

References

[1] WU Z B, JIANG M J, YANG C J, et al. Extrusion failure analysis and structural optimization of sealing ring of pulley under pressure[J]. Lubrication Engineering, 2024, 49(03):143-153.

ISSN: 2688-8645

[2] TAN J, YANG W M, DING Y M, et al. Finite element analysis of the sealing performance of O-ring seal structure[J]. Lubrication Engineering, 2006, (09):65-69.

[3] GUAN W J, DU Q G, LIU P Q. Finite element analysis of the sealing performance of rubber O-ring[J]. Lubrication Engineering,2012, 37(06):60-64.

[4] ZHANG Q, JIN G. Finite element analysis of contact pressure on O-ring[J]. Lubrication Engineering, 2010,35(02):80-83.

[5] YANG B, HUANG L, DING J P, et al. Simulation of O-ring seal eccentricity[J]. Lubrication Engineering, 2021,46(11):27-33.

[6] WU Z B, KOU T, ZHU X C, et al. Simulation analysis of the sealing performance of rubber O-ring of tooth wheel arill bit bearing under unaligned working condition[J]. Lubrication Engineering, 1-12[2025-08-30].

[7] XIN Y F. Research on sealing mechanism and influence mechanism of sealing ring under eccentric and off-load conditions.[D] Yan San University, 2024.

[8] LIANG B L, YANG X, WANG Z L, et al. Influence of Randomness in Rubber Materials Parameters on the Reliability of Rubber O-Ring Seal[J]. MATERIALS, 2019,12:1-12.